

The Dynamics and Control of a Haptic Interface Device

H. Kazerooni and Ming-Guo Her, *Member, IEEE*

Abstract—Haptic Interface Devices are machines that are controlled by the human arm contact forces. These devices are necessary elements of virtual reality machines. These devices may be programmed to give the human arm the sensation of forces associated with various arbitrary maneuvers. As examples, these devices can give the human the sensation that he/she is maneuvering a mass, or pushing onto a spring or a damper. In general, these devices may be programmed for any trajectory-dependent force. To illustrate and verify the analysis of these machines, a two-degree-of-freedom electrically-powered haptic interface device was designed and built at the Human Engineering Laboratory (HEL) of the University of California-Berkeley.

I. NOMENCLATURE

ALL MATRICES AND VECTORS are $n \times n$ and $n \times 1$, where n is the number of degrees of freedom for the haptic interface device. The Laplace arguments of the transfer functions and the arguments of nonlinear operators are shown in the nomenclature but are dropped in the text.

C : DC feedback gain
 $E(p)$: a nonlinear vector operator; representing the environment¹ dynamics
 $E_0(s)$: a matrix; representing the linear portion of the environment dynamics
 f_e : a vector; the force imposed on the haptic interface device by the environment
 f_{ext} : a vector; any force imposed on the environment by external objects other than the device or the human arm
 f_h : a vector; the force imposed on the haptic interface device by a human arm
 f_h^* : a vector; the force imposed on the haptic interface device by the human arm at no-environment condition
 f_i : a vector; the intended force applied by the human arm, as commanded by the central nervous system
 $G(s)$: a matrix; the closed loop transfer function mapping desired position, p_{des} to device endpoint position, p
 G_a : muscle activation dynamics
 G_{ens} : a matrix; transfer function relating neural input to human arm configuration
 G_f : neural feedback dynamics

G_p : muscular contraction and passive tissue dynamics
 $H(p)$: a nonlinear operator representing human arm dynamics, impedance
 $H_0(s)$: a matrix representing the linear portion of the human arm dynamics
 $K(s)$: a matrix representing the stability controller
 m : descending neural commands
 n : the degrees of freedom of the haptic interface device
 p : a vector; the actual endpoint position of the haptic interface device
 p_{des} : a vector; the desired endpoint position of the haptic interface device
 $R(s)$: a matrix; the performance index
 s : the Laplace operator (sec^{-1})
 $S_e(s)$: a matrix; the sensitivity function mapping environment force, f_e , to the endpoint position of the haptic interface device, p
 $S_h(s)$: a matrix; the sensitivity function mapping human force, f_h , to the position of the haptic interface device, p
 u_n : a vector; the human muscle force which initiates a maneuver
 $\alpha(s)$: a matrix representing the linear controller operating on the human arm force, f_h
 $\Delta(p)$: a vector operator representing the nonlinear dynamics in the human and the environment
 λ : scalar

II. MOTIVATION AND INTRODUCTION

This article describes the design, dynamics and control of powered haptic interface devices. Fig. 1 shows one example of such a device: a two-degree-of-freedom haptic interface device built at the University of California at Berkeley. This device can be programmed to impose arbitrary trajectory-dependent forces on the human arm. The human maneuvers the device in a vertical two-dimensional plane by holding a handle at the device endpoint. (More description on the experimental device of Fig. 1 is given in Section VI.)

Three elements contribute to the dynamics of these systems: the human arm, the haptic interface device and the environment being maneuvered. The motion commands to the haptic interface device are taken directly from two sets of interaction forces: one between the human and the device and one between the environment and the device. While the human interaction

¹ In this article, the word environment has been used to represent any object being manipulated or pushed by the haptic device.

Manuscript received March 2, 1992; revised February 11, 1993.
 H. Kazerooni is with the Mechanical Engineering Department, University of California, Berkeley, CA 94720.

M.-G. Her is with the Department of Mechanical Engineering, Tatung Institute of Technology, Taipei, Taiwan.
 IEEE Log Number 9402206.

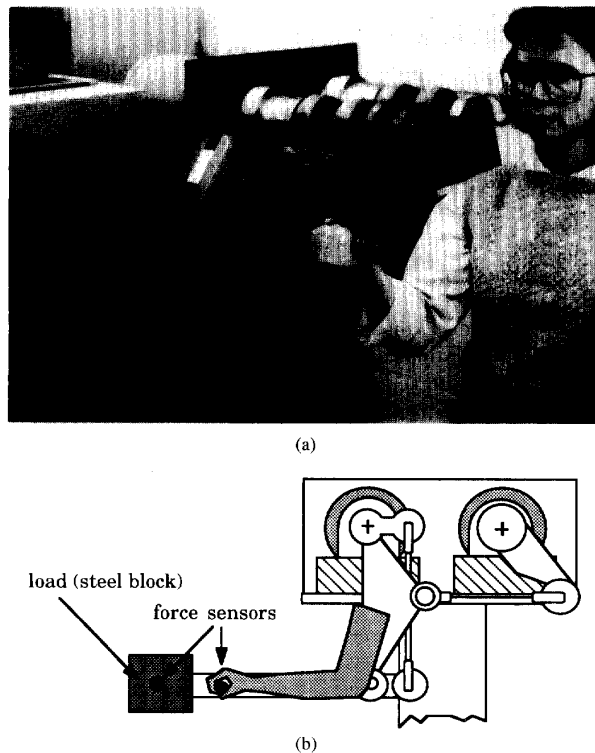


Fig. 1. (a) The two-degree-of-freedom general purpose haptic interface built at the University of California, Berkeley. The human maneuvers the device in a vertical two-dimensional plane by holding a handle at the haptic interface endpoint. The haptic interface controller translates the two measured interaction forces into a motion command for the device so that the force imposed on the human by the device is an arbitrary function of the force imposed on the device endpoint by the environment. (b) The haptic interface mechanism.

force helps move the device, the environment interaction force impedes the device motion.

The controller of the haptic interface device translates the two measured interaction forces into a motion command for the device so that the force imposed on the human by the device is an arbitrary function of the force imposed on the device endpoint by the environment. This functionality can be expressed by designers as a set of linear differential equations. In a very simple example, if this functionality is expressed as a constant number, then the force the human feels is linearly proportional to the force that the environment imposes on the haptic interface device. This simple functionality may be programmed into the controller. In a more complex example, the device may be programmed so the forces the human feels are similar to forces associated with maneuvering the mass held by various springs and dampers. (The general form of the haptic interface performance is expressed mathematically in Section IV.)

As is seen from Fig. 1, the haptic interface device is in physical contact with both the human and the environment. Forces between the human and the device and forces between the environment and the device are measured and processed so the human senses a desired force. Fig. 2 symbolically depicts

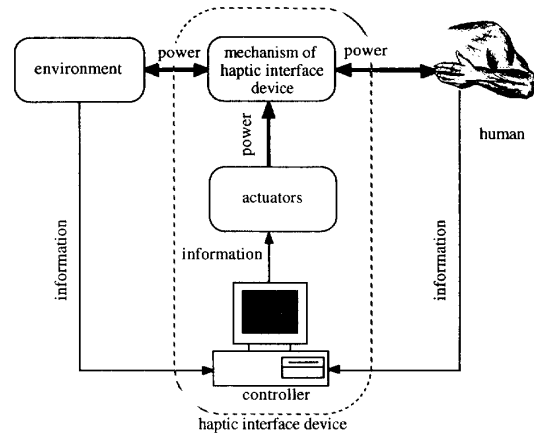


Fig. 2. The motion of a haptic interface device is subject to forces from the human and from the environment. These forces create two paths for power transfer to the device: one from the human and one from the environment. These forces are also measured and processed for proper maneuvering of the device. These measured signals create two paths for information transfer to the haptic interface device: one from the human and one from the environment.

the communication paths between the human, haptic interface device and environment. With respect to Fig. 2, the following statements describe the fundamental features of the haptic interface device.

- 1) The haptic interface device is powered and consists of: 1) hardware (electromechanical), and 2) a computer for information processing and control.
- 2) The environment position is the same as the device endpoint position.
- 3) The motion of the haptic interface device is subject to forces from the human and from the environment which create two paths for power transfer to the device: one from the human and one from the environment. No other sources impose forces on the device.
- 4) Forces between the human and the device and forces between the environment and the device are measured and processed. These measured signals create two paths for information transfer to the haptic interface device: one from the human and one from the environment. No information signals from other sources (such as joysticks, pushbuttons or keyboards) are used to drive the haptic interface. (See [11], [25] and [28] concerning the significance of power and information signals paths in human machine systems)

This effort determines the principles associated with the analysis and design of haptic interface devices which allow programming the arbitrary specification of the forces on the human arm. More specifically, Section III describes the dynamic behaviors of the system components and the human. Section IV discusses the control of haptic interface devices and develops a criteria to ensure achievement of the performance specification. Section V derives a condition that ensures closed-loop stability when users with various strengths use these devices. Section VI provides the experimental results on the two-degree-of-freedom direct-drive electric haptic interface device.

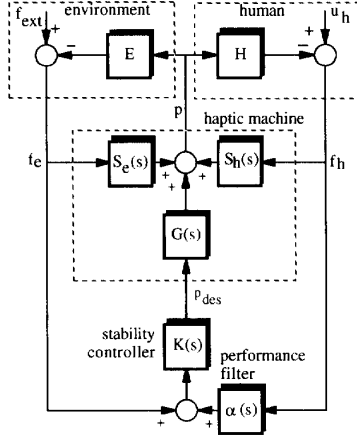


Fig. 3. The overall block diagram for the haptic interface device. The device dynamics, which are linearized by the primary stabilizing controller, are represented by G , S_h , and S_e . The human and the environment dynamics are represented by two nonlinear operators H and E . Two linear controllers α and K modulate the forces f_h and f_e .

III. DYNAMICS

This section describes the dynamic behavior of the haptic interface device and the human arm, which are combined in Fig. 3.

It is assumed that the haptic interface device primarily has a closed-loop position controller, which is called the *primary stabilizing controller*. The resulting closed-loop system is called the *primary closed-loop system*. The selection of the primary stabilizing controller is not discussed here; a variety of controllers may be used to stabilize the device in the presence of uncertainties and nonlinearities. These controllers result in an “almost” uncoupled and linearized closed-loop behavior for the device within a certain frequency range [16], [29]. The primary stabilizing controller has the following features:

- 1) When the human separates his/her hand from the haptic device in emergency situations, the primary stabilizing controller must hold the device stationary at the configuration at which the human arm separated from the device. The primary stabilizing controller guarantees the device stability when the human is not maneuvering the device.
- 2) The primary stabilizing controller of the haptic interface device minimizes the uncertainties in the device dynamics and creates a more definite and linear dynamic model for the device. Therefore, it is assumed that the dynamics of the haptic interface device are linearized by the primary stabilizing controller over a range of operation. This linear model may then be used to design other controllers that operate on forces f_h (human force) and f_e (environment force). For the experimental device employed in this research effort, the computed-torque method along with a PD controller [1], [2] is used as the primary stabilizing controller to create a more definite and linear dynamics for the device.
- 3) The human arm dynamics, unlike the haptic device dynamics, change significantly with each human and

also within one person over time [10], [25]. The design of the primary stabilizing controller must let the designer deal with the effect of the device uncertainties without concern for the dynamics of the human operator.

Regardless of the type of primary stabilizing controller, the position of the haptic interface device, p , results from two inputs: 1) the desired position command, p_{des} and 2) the forces imposed on the haptic interface device. The transfer function matrix G represents the primary closed-loop position system which maps p_{des} to the device position, p . Two forces are imposed on the device: f_h is imposed by the human, and f_e is imposed by the environment. S_h , the haptic device sensitivity transfer function, maps the human force, f_h , onto the device position, p . Similarly, S_e , the haptic device sensitivity transfer function, maps the environment force, f_e , onto the device position, p . If the primary stabilizing controller is designed so that S_h and S_e are small, the haptic device has only a small response to the imposed forces f_h and f_e . A high gain controller in the primary stabilizing controller results in small S_h and S_e and consequently a small device response to f_h and f_e . Using G , S_e and S_h , (1) represents the dynamic behavior of the haptic interface device.

$$p = Gp_{des} + S_h f_h + S_e f_e \quad (1)$$

The middle part of the block diagram in Fig. 3 represents the haptic interface model (i.e., (1)) interacting with the human and the environment. The upper right part of the block diagram represents the human arm dynamics. The human arm’s force on the haptic interface, f_h , is a function of both the human muscle forces, u_h , and the position of the device, p . Thus, the device motion may be considered to be a position disturbance occurring on the force-controlled human arm. If the device is stationary (i.e., $p = 0$), then the force imposed on the device is solely a function of the human muscle force command produced by the central nervous system. Conversely, if the haptic interface device is in motion and $u_h = 0$, then the force imposed on the device is solely a function of the human arm impedance, $H(p)$. H is a nonlinear operator representing the human arm impedance as a function of the human arm configuration; H is determined primarily by the physical properties of the human arm [4], [24], [30]. Based on the above, (2) represents a dynamic model of the human arm.

$$f_h = u_h - H(p) \quad (2)$$

The exact form of u_h is not known other than it results from human muscle force on the haptic interface device.² A simple study of how the central nervous system generates the desired force command u_h is given in [5], [7]. The experimental procedure to measure H from various subjects is given in Section VI.

The environment force impedes the motion of the haptic interface device. The haptic interface controller translates the two measured interaction forces into a motion command for the device to create a desired relationship between the human

²The internal structure of H does not play a significant role in the control technique described here; a brief description of the internal structure of H is given in the Appendix as a support for the selected form for (2). Readers may proceed, if this description seems peripheral.

forces and the environment forces. E is a nonlinear operator representing the environment dynamics. f_{ext} is the equivalent of all the external forces imposed on the environment which do not depend on p and other system variables. Equation (3) provides a general expression for the force imposed on the haptic interface device, f_e , as a function of p .

$$f_e = -E(p) + f_{\text{ext}} \quad (3)$$

In the example of accelerating a point mass m along a horizontal line, the environment force, f_e , can be characterized by $f_e = ms^2p$. In this case $E = ms^2$ and $f_{\text{ext}} = 0$ where p is the mass position and s is the Laplace operator. If the mass is large and cannot be represented by a point mass, then E can be calculated using Lagrangian formulation.

The diagram of Fig. 3 includes two linear controllers, $\alpha(s)$ and $K(s)$, which modulate the forces f_h and f_e . α and K (which are implemented on a computer) must be designed to produce a desired performance in the haptic interface device; this is described in the next section. As the Fig. 3 block diagram shows, the performance filter α lets designers choose the appropriate performance for the haptic interface device and the stability filter K (which operates on both f_h and f_e) guarantees the system stability when the device is used by people with various arm impedances (strengths). One may also think of K and α as two controllers that produce compliance in response to the human forces and environment forces; this control method is referred to as "force control" and "compliant motion control" in robotics literature [15], [19]–[21], [23], [26], [31].

IV. CONTROL

To understand the role of controllers α and K , assume for a moment that neither controller is included in the system. If the commanded position, p_{des} , the human muscle forces, u_h , and the external forces, f_{ext} , all equal zero, then the device position, p , equals zero and no motion is transmitted to the environment. This is the case when the human is holding the haptic interface device without intending to maneuver it. If the human decides to initiate a maneuver, then u_h takes on a nonzero value and a device motion develops from f_h . The resulting motion is small if S_h is small. In other words, the human may not have enough strength to overcome the device primary closed-loop controller.

To increase the human's effective strength, the device effective sensitivity to f_h must be increased by measuring the human force, f_h , and passing it through the controllers α and K . Fig. 3 shows that $GK\alpha$, parallel with S_h , increases the effective sensitivity of the device to f_h . To retain a sense of the environment in the device operation, the environment force, f_e , is also measured and passed through K . This produces the loop GK , parallel with S_e , which increases the effective sensitivity of the device to f_e . The output of K is applied to the device as a desired position command, p_{des} . K and α must be chosen to ensure the stability and performance of the closed-loop haptic interface system. The proper choice of K

and α achieves a desired ratio of human force to environment force and guarantees the closed-loop stability of Fig. 3.³

Next, the following question is addressed: how should the haptic interface device perform in a particular maneuver? In specifying the system's performance, the designers decree the important criteria which must be met for the successful completion of a maneuver. Also in the performance specification, the designers describe the haptic device behavior they find desirable if stability can be maintained. Performance goals and stability requirements do conflict. As is clarified in the next section, the designers must balance this trade-off to develop a machine that both performs well and is guaranteed to be stable.

The following example illustrates a simple specification for the performance of a haptic interface device. The human uses the device to maneuver a free mass in space. A reasonable performance specification for this example would state the level of amplification of the human force which is applied to the free mass. If the force amplification is large, a small force applied by the human results in a large force being applied to the free mass. If the amplification is small, a small force applied by the human results in a small force being applied to the free mass. Consequently, if the amplification is large, the human "feels" only a small percentage of the interaction force with the free mass. Most importantly, the human still retains a sensation of the dynamic characteristics of the free mass, yet the mass essentially "feels" lighter or heavier as required.

With these heuristic ideas of system performance, the performance of the haptic interface device is captured in (4) where f_h^* is the human force applied to maneuver the device when no environment is present. R is the *performance matrix* and $[0, \omega_p]$ is the frequency range of the human arm motion.

$$(f_h - f_h^*) = -Rf_e \quad \text{for all } \omega \in [0, \omega_p] \quad (4)$$

Equality (4) guarantees that $(f_h - f_h^*)$, the portion of the human force that is actually applied to maneuver the environment, is proportional to the environment force, f_e . The performance matrix R is an $n \times n$ linear transfer function matrix. Suppose R is chosen as a diagonal matrix with all members having magnitudes smaller than unity over some bounded frequency range. Then the human force is smaller than the environment force by a factor of R . Suppose R is chosen as a diagonal matrix with all members having magnitudes greater than unity. Then the human force is larger than the environment force by a factor of R . In a more complex example, the transfer function matrix R may be selected to represent linear passive dynamic systems (i.e., combinations of dampers, springs and masses).

By inspecting Fig. 3, the position of the haptic interface device is written as a function of f_h and f_e .

$$p = (GK\alpha + S_h)f_h + (GK + S_e)f_e \quad (5)$$

Now suppose that the human maneuvers the haptic interface device through the same trajectory indicated by p in (5) except without any environment. The no-environment human force,

³Another way of interpreting K and α is as follows. K is a linear controller that servos the difference between (f_e) and (αf_h) to zero.

f_h^* , is then obtained by inspection of Fig. 3 where $E = 0$ and $f_{\text{ext}} = 0$:

$$p = (GK\alpha + S_h)f_h^* \quad (6)$$

Equating the trajectories from (5) and (6) results in (7).

$$(f_h - f_h^*) = -(GK\alpha + S_h)^{-1}(GK + S_e)f_e \quad (7)$$

Comparing (4) and (7) shows that to guarantee the performance represented by R in (4), inequality (8) must be satisfied.

$$\sigma_{\max}[(GK\alpha + S_h)^{-1}(GK + S_e) - R] < \varepsilon \text{ for all } \omega \in [0, \omega_p] \quad (8)$$

where σ_{\max} represents the maximum singular value. ε represents a small positive number chosen by the designer to denote the degree of precision required for the specified performance within the frequencies $[0, \omega_p]$. A small value for ε (e.g., 0.01) indicates a close proximity of the actual system performance to the specified performance R (e.g., within a 1% error). Note that the human arm and environment dynamics, H and E , are absent from inequality (8). Thus, achievement of the specified performance R depends only on the dynamics of the haptic interface device (G, S_e, S_h) and on the controllers (K, α) and not on the particular human operator and environment.

Satisfaction of inequality (8) guarantees that the performance defined by (4) is achieved with precision ε . Therefore, the goal is to select K and α so condition (8) is satisfied. Assuming that R is selected so R^{-1} always exists, α is chosen to be equal to R^{-1} . (This unexpected choice for α results from investigations of several design methods). Substituting R^{-1} for α in inequality (8) shows that any K which satisfies inequality (9) also satisfies inequality 8.

$$\sigma_{\max}(GK) > \frac{\sigma_{\max}(S_e - S_h R)\sigma_{\max}(R)}{\varepsilon} \text{ for all } \omega \in [0, \omega_p] \quad (9)$$

Inequality (9) suggests that, since ε is a small number, the designer must choose K to be a transfer function matrix with large magnitude to satisfy inequality (9) for frequencies $\omega \in [0, \omega_p]$ and for a given ε, R, S_h and S_e . The smaller ε is chosen to be, the larger K must be to achieve the desired performance. K may not be arbitrarily very large: the choice of K must also guarantee the closed-loop stability of the system shown in Fig. 3, as discussed in the next section.

V. STABILITY

It has been shown that, to achieve the system performance indicated by R , α must be equal to R^{-1} and K must be a large transfer function matrix satisfying inequality (9). However, the designers must realize that the closed-loop system of Fig. 3 must remain stable for these choices of α and K . The selection of K is particularly important since H and E generally contain nonlinear dynamic components. For example, the human arm impedance H changes from person to person and also within one person over time. The environment dynamics E is also a nonlinear element as discussed earlier. Compared to the human arm and environment dynamics, the haptic interface dynamics (G, S_e, S_h) are generally well-defined due to the primary stabilizing controller. Consequently, this analysis focuses on

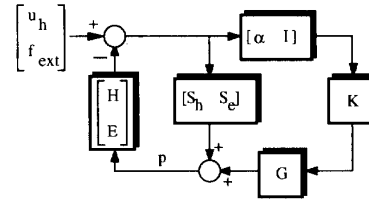


Fig. 4. Simplified block diagram of Fig. 3. I is a unity matrix.

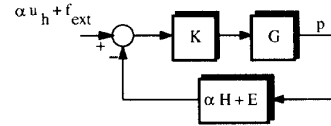


Fig. 5. In systems with very small sensitivity transfer functions, S_e and S_h are much smaller than G and their effect on the overall system dynamics is negligible.

designing a stabilizing controller K in the presence of all bounded variations of the nonlinear operators H and E with G, S_e and S_h being known and linear dynamics. The following questions illuminate our approach to the design of K .

In designing K , is it possible to work with a human arm and a environment with linear dynamics (represented by H_0 and E_0) instead of the nonlinear dynamics represented by operators H and E ? If the answer is *yes*, then what properties should H_0 and E_0 have so that the designed K both satisfies inequality (9) and stabilizes the Fig. 3 system in the presence of a family of nonlinear operators H and E ?

The block diagram of Fig. 3 is transformed into the block diagram of Fig. 4 in order to group the nonlinear operators, H and E , into one block on the diagram.

S_h and S_e represent the sensitivities of the haptic device position to the human and environment forces. G, S_h and S_e depend on the nature of the machine's primary stabilizing controller. If a primary stabilizing controller with a large position loop-gain or integral control is chosen to insure small steady state errors, then S_h and S_e are extremely small compared to G , approaching zero at steady-state. Prototype haptic interface designs have produced sensitivities on the order of 10^3 to 10^6 times smaller than G [12]. If the actuators of the haptic device are non-backdrivable, as in systems with geared large transmission ratios, then S_h and S_e are zero regardless of how carefully the haptic interface's primary stabilizing controller is chosen. Since S_h and S_e are typically much smaller than G , their effect on the overall system dynamics is negligible. Therefore S_h and S_e are disregarded in the following stability analysis. Fig. 5 presents the resulting simplified stability diagram. Note that the stacked nature of the input signal, the human and environment dynamics in Fig. 4 are now reduced to single entities where $(\alpha H + E)$ is a nonlinear operator and K and G are transfer function matrices.

If H_0 and E_0 are assumed to represent a particular set of linear human and environment dynamics, (10) represents the general form of H and E where Δ is the stable nonlinear part of the dynamics. In cases where the nonlinear dynamics may

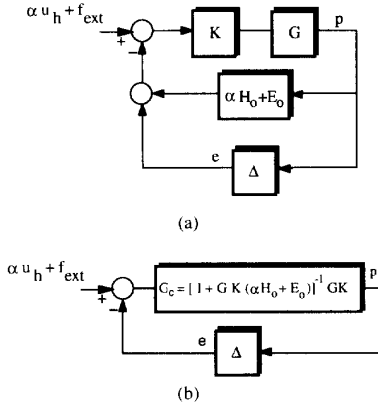


Fig. 6. Δ is the stable nonlinear operator representing the nonlinear human and environment dynamics.

not be directly separated from the linear dynamics, an estimate of H_0 and E_0 must be formed from experiments such as those in Section V.

$$\alpha H(p) + E(p) = [\alpha H_0 + E_0] p + \Delta(p) \quad (10)$$

Note that $[\alpha H_0 + E_0]$ is a transfer function matrix operating on p . The block diagram of Fig. 5 can be transformed into the block diagram of Fig. 6 which separates the nonlinear term Δ from the linear terms $[\alpha H_0 + E_0]$.

With respect to Fig. 6, the design of K is approached as follows.

A stabilizing controller K must be designed for a set of linear H_0 and E_0 so that the closed-loop system of Fig. 6 remains stable and inequality (9) (indicating the performance) is satisfied.⁴ This controller must guarantee enough stability robustness for all bounded values of H and E . Therefore the goal is to find a particular class of H_0 and E_0 and a stabilizing controller K that together yield the largest stability robustness for a given largest Δ .

Equation (11) represents the forward loop in Fig. 6(b).

$$G_c = [I + GK(\alpha H_0 + E_0)]^{-1} GK \quad (11)$$

The stability of each element in Fig. 6(b) is described by inequalities (12), (13), and (14):

$$\|\alpha u_h + f_{ext}\|_\infty \leq \beta_{in} < \infty \quad \text{"input is } L_\infty \text{ bounded"} \quad (12)$$

$$\|e\|_\infty \leq \lambda_\Delta \|p\|_\infty + \beta_\Delta \quad \text{"}\Delta \text{ is } L_\infty \text{ stable"} \quad (13)$$

$$\|p\|_\infty \leq \lambda_{G_c} \|e\|_\infty + \beta_{G_c} \quad \text{"}G_c \text{ is } L_\infty \text{ stable"} \quad (14)$$

λ and β are finite positive constants that indicate L_∞ stable mappings. The closed-loop system of Fig. 6 is L_∞ stable if the norm of the output p is bounded. According to the Small Gain Theorem [6], this is guaranteed if inequality (15) is satisfied.⁵

$$\lambda_{G_c} \lambda_\Delta < 1 \quad (15)$$

⁴ Note that the performance as defined by inequality (9) is independent of H_0 and E_0 .

⁵ Since G_c , by definition, is linear and L_∞ -stable, λ_{G_c} is defined as the A -norm of the impulse response of G_c and β_{G_c} equals zero.

The human arm impedance H changes from person to person and also within one person over time. This leads to large variations for λ_Δ . To obtain an intuitive feel for the stability condition in inequality (15), evaluation of inequality (15) within the operating range of the haptic interface system is useful. If K is designed as a very large transfer function in order to guarantee system performance (as prescribed by inequality (9)), then (11), within the controller bandwidth, may be approximated by:

$$G_c \approx [\alpha H_0 + E_0]^{-1} \quad \text{for all } \omega \in [0, \omega_p] \quad (16)$$

One must choose the largest environment that an haptic interface device can manipulate to be E_0 , the strongest human impedance to be H_0 , and the greatest force amplification as a performance specification to be α_{max} . Then, $[\alpha_{max} H_0 + E_0]$ will be larger, and G_c and consequently λ_{G_c} will be smaller. If λ_{G_c} is smaller, then, according to inequality (15), λ_Δ takes on larger values. In other words, if the largest values of α , H and E are used to design a stabilizing K (i.e., one that guarantees inequality (9)), then the closed-loop system will remain stable in the presence of the large variations of human and environment dynamics represented by a large λ_Δ .

Inequality (9) also teaches that a large K is needed to guarantee achievement of the system performance. Inspection of Fig. 5 shows that choosing a large $[\alpha_{max} H_0 + E_0]$ for stability robustness (as discussed above) restricts the designer's choices for a large K . This is true because large values for both K and $[\alpha_{max} H_0 + E_0]$ may cause a large loop gain and consequently an unstable system in Fig. 5. Therefore, although choosing a large value for $[\alpha_{max} H_0 + E_0]$ leads to stability robustness, it may prohibit the designer's choosing a large K to satisfy the performance specification in inequality (9). Thus, the better understood the environment and human dynamics are, the smaller λ_Δ will be; this leaves more room to increase K and gain more precision in achieving the desired performance as stated by inequality (9). Similar stability analysis is given for robotic compliant maneuvers and force control systems [13], [14].

VI. EXPERIMENTAL ANALYSIS

A. Haptic Interface

The prototype two-degree-of-freedom electric direct-drive haptic interface device (Fig. 1 and Fig. 7) is used to verify experimentally the theoretical predictions of the system stability and performance.

Fig. 7 shows the seven-bar-linkage mechanism used for our prototype laboratory haptic interface device. This device has two degrees of freedom corresponding to a shoulder and an elbow. The addition of a third degree of freedom is also possible in this design: either rotation about a vertical axis or roll about a horizontal fore-aft axis. Force sensors are mounted at the human-machine and machine-environment interfaces. Motor 2 rotates link 4 causing the main arm (link 6) to move up and down via a four-bar linkage (links 4, 5, 6, and 3 as the ground link). In another four-bar linkage (links 1, 2, 3, and 7), motor 1 rotates link 1 causing the follower link

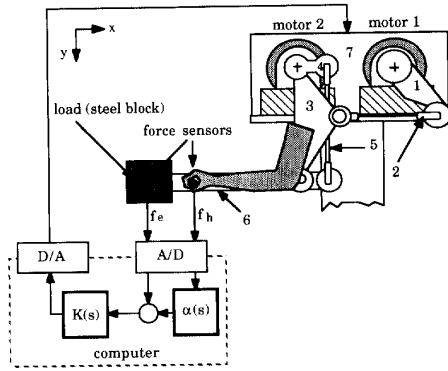


Fig. 7. The experimental haptic interface used to verify the analysis.

(link 3) and the main arm (link 6) to move in and out. Both motors 1 and 2 are connected to bracket 7 which is mounted on a platform at the same height as the human shoulder. A gripper is mounted on link 6 where the operator force, f_h , is measured along two directions. When the human holds onto the gripper, his/her upper arm parallels link 3 and his lower arm parallels link 6. The materials and the dimensions of the device components are chosen to preserve the structural-dynamic integrity of the haptic interface. (References [12], [17], [18], [22] describe some of the fundamental design issues associated with robotic systems maneuvered by humans). Each link is machined as one solid piece rather than as an assembly of smaller parts. Link 1, 3, 6 are made of high strength 7075 aluminum alloy to reduce the weight of the haptic interface device. Link 2, 4, 5 are made of steel to fit in limited design space.

The mechanism is safe in the sense that the human's head and shoulders stand clear of the mechanism workspace. Two limit switches are mounted on the housings and shafts of the actuators so the actuators are inactive outside of the human arm workspace. Mechanical stops are mounted on three various links to prevent the motion of the mechanism beyond the permitted workspace. We have also developed software to monitor the states of the system. The angular positions, velocities and acceleration of the actuators, as well as the contact forces between the human arm and the device, form the data for this software. If there is a substantial difference between the measured data and the permitted values, the system shuts off.

Because of the actuators' wide bandwidth dynamics, the actuator dynamics of the haptic interface device are negligible. The machine's primary closed-loop controller measures angular position using resolvers. A linear model for the primary closed-loop system in a Cartesian coordinate frame⁶ is derived with a computed torque method used in conjunction with a simple PD controller. Employing this primary controller, the haptic interface closed-loop transfer function G in the Cartesian coordinate frame along the x - and y -directions of

⁶For brevity, the selection of primary stabilizing compensator (computer torque and PD controller) is not discussed here. See [29] for detailed description of such control method.

Fig. 7 is:

$$G(s) = \frac{1.2516s + 2.079}{0.002s^3 + s^2 + 1.2516s + 2.079} \text{ Newton/Newton} \quad (17)$$

B. Human Arm

The human arm dynamics do not affect performance (defined by inequality (9)) but do play a major role in system stability. Several experiments were conducted to measure the human arm impedance H . Then the largest of these impedances was chosen to be H_0 in the stability analysis. In the experiments to determine the largest H , the subject grasped a handle on the haptic interface device. The device was commanded to oscillate via sinusoidal functions. The frequency and amplitude of oscillation were changed continuously by the software. (See [3] for more detailed information about the nature of these experiments.) The human operator tried to move his/her hand to follow the device so that zero contact force would be maintained between the hand and the device. Since the frequency of operation changes continuously and feels rather random, the operator could not predict the frequency of motion.

The human arm, when trying to maintain zero contact forces on the handle, cannot keep up with the high-frequency motion of the haptic interface device. At high frequencies, the forearm is moved without the benefit of active feedback from the central nervous system. In other words, in the high frequency region, we observe that the impedance behaves like a purely inertial mass. Thus, large contact forces and consequently a large H are expected at high frequencies. Since this force is equal to the product of the haptic interface acceleration and human arm inertia (Newton's Second Law), at least a Second-order transfer function is expected for H at high frequencies. At low frequencies (in particular at dc), the operator can follow the device motion comfortably and can establish almost constant contact forces between the hand and the haptic interface. Thus, small contact forces at all device positions and consequently a constant transfer function for H are expected at low frequencies.

Fig. 8 shows the experimental values and the fitted transfer functions for two different experiments. In the first experiment (shown by plus signs), the subject holds the device handle loosely. In the second experiment (shown by squares), the subject holds the device handle very tightly. At low frequencies, the human arm impedance is smaller when the subject holds the handle loosely than when the subject holds the handle very tightly. Observing the slope of 40 db/dec for both plots show an inertial behavior at high frequencies. The largest impedance (shown by squares) is chosen for use in the stability analysis.

$$H_0 = 12.1 \left(\frac{s^2}{43.69} + \frac{s}{5.08} + 1 \right) \text{ lbf/ft} \quad (18)$$

C. Mass

The mass that was installed on the haptic interface endpoint is 33.82 N at a distance of 0.5 m from the elbow joint as shown in Fig. 7. The handle was mounted at 0.3 m from the elbow joint. Since the mass and human hand are placed in different

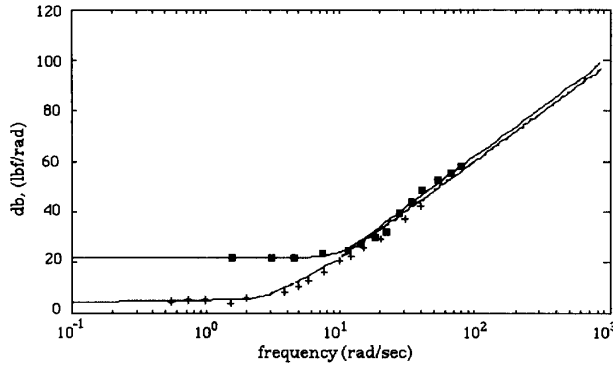


Fig. 8. The Experimental and theoretical plot of H ; in the first experiment (shown by plus signs), the subject holds the device handle loosely. In the second experiment (shown by squares), the subject holds the device handle very tightly.

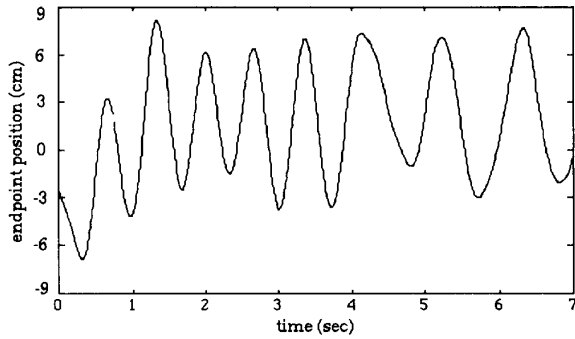


Fig. 9. The haptic device motion along the x -direction.

locations, the equivalent of the heaviest mass dynamics needed for stability analysis is represented by (19).

$$E_0 = 9.08s^2 \quad \text{newton/meter} \quad (19)$$

D. Performance

Matrix R in (20) is chosen as the performance matrix in the Cartesian coordinate frame.

$$R^{-1} = \alpha = \begin{pmatrix} 8 & 0 \\ 0 & 5 \end{pmatrix} \quad (20)$$

The above performance specification has force amplifications of eight times in the x -direction and five times in the y -direction.

Figs. 9 and 10 depict the history of the haptic device position, x and y , as a function of time in an experiment where the human operator maneuvers the device irregularly (i.e., randomly). Fig. 11 shows the experimental values of the human force f_h in the x -direction. Fig. 12 shows two graphs versus time, $(f_h - f_h^*)$ and f_e along the x -direction where the environment force f_e is more than $(f_h - f_h^*)$ by a factor of 8. This figure also shows the simulated value of $(f_h - f_h^*)$ which is calculated from αf_e where f_e is the experimental value of the environment force. Fig. 13 shows f_e versus $(f_h - f_h^*)$ along the x -direction where the slope of -8 represents the force amplification by a factor of 8 along the x -direction.

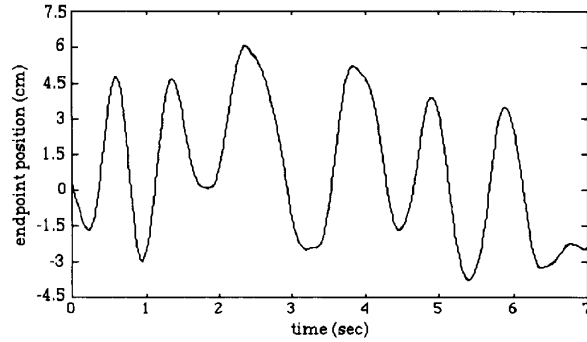


Fig. 10. The haptic device motion along the y -direction.

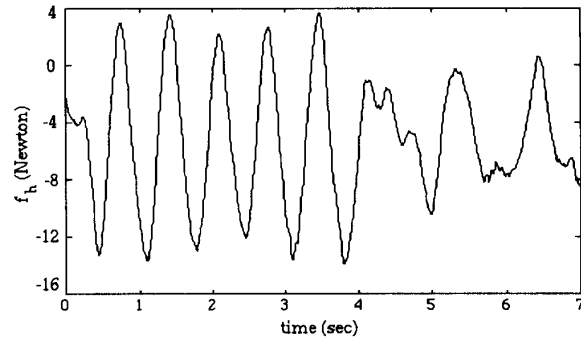


Fig. 11. The human force f_h along the x -direction at $\alpha = -8$.

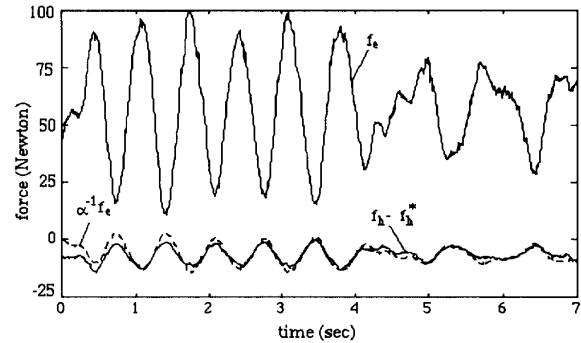


Fig. 12. f_e and $(f_h - f_h^*)$ along the x -direction at $\alpha = -8$.

Figs. 14, 15, and 16 are similar to Figs. 11, 12, and 13, except that they have a force amplification of 5 in the y -direction. Fig. 14 presents the experimental values of the human force f_h in the y -direction. Fig. 15 shows two graphs versus time, $(f_h - f_h^*)$ and f_e along the y -direction where the environment force, f_e , is more than $(f_h - f_h^*)$ by a factor of 5. Fig. 16 shows f_e versus $(f_h - f_h^*)$ along the y -direction where the slope of -5 represents the force amplification by a factor of 5 in the y -direction. This experiment also shows that the larger α is, the more precision is gained in the achievement of the performance.

Figs. 17 and 18 show the haptic interface position and human force in the y -direction when $\alpha = -19$ which violates the stability criteria in inequality (9).

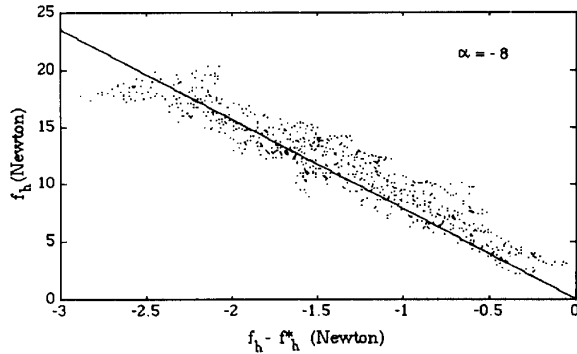


Fig. 13. f_c versus $f_h - f_h^*$ along the x -direction at $\alpha = -8$.

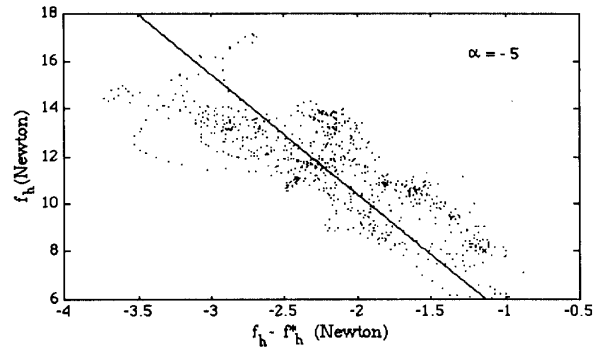


Fig. 16. f_c versus $(f_h - f_h^*)$ along the y -direction at $\alpha = -5$.

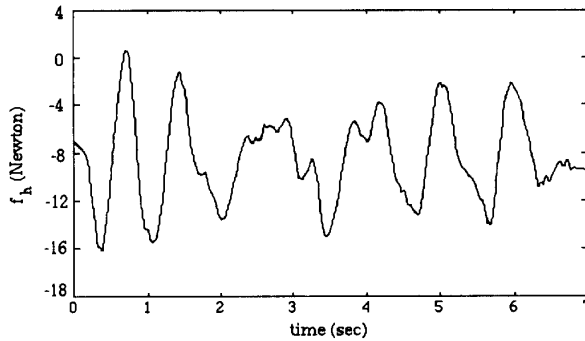


Fig. 14. The human force f_h along the y -direction at $\alpha = -5$.

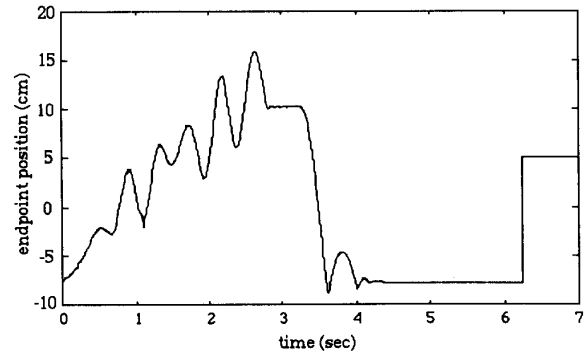


Fig. 17. The haptic interface device motion over time along the y -direction at $\alpha = -19$.

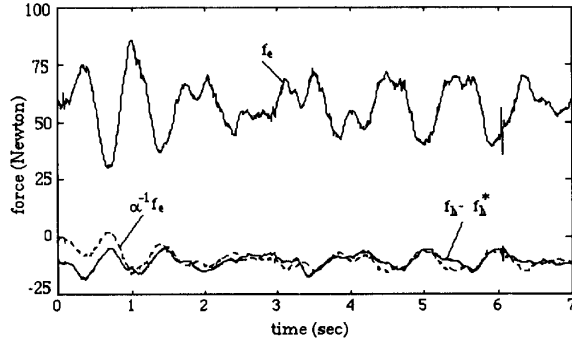


Fig. 15. f_c and $(f_h - f_h^*)$ along the y -direction at $\alpha = -5$.

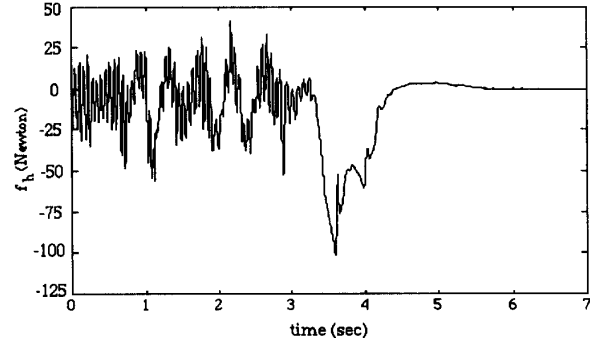


Fig. 18. The human force f_h along the y -direction at $\alpha = -19$. The haptic interface device is unstable.

VII. SUMMARY AND CONCLUSION

This article describes the design and dynamics of powered haptic interfaces. These devices may be programmed to give the human arm the sensation of forces associated with various arbitrary maneuvers. System performance is defined as a linear relationship between the human force and the environment force. A condition for stability of the total system (haptic interface device, human arm and environment) is derived and, through experimentation, the sufficiency of this condition is demonstrated. A two-degree-of-freedom electric haptic interface has been built for experimental verification of the analysis.

APPENDIX

A. Dynamic Behavior of the Human Arm

We avoid attributing a particular class of dynamic behaviors to constrained movements of the human arm, as it is not clear whether the arm behaves as a force or a position control system in constrained motions. Maneuvering our hands in a stream of water from one point to another target point, while struggling with the water current, is an example that shows the human arm can work as a position control in a constrained space and can continuously accept a position or velocity command from the central nervous system. Alternatively, pushing a

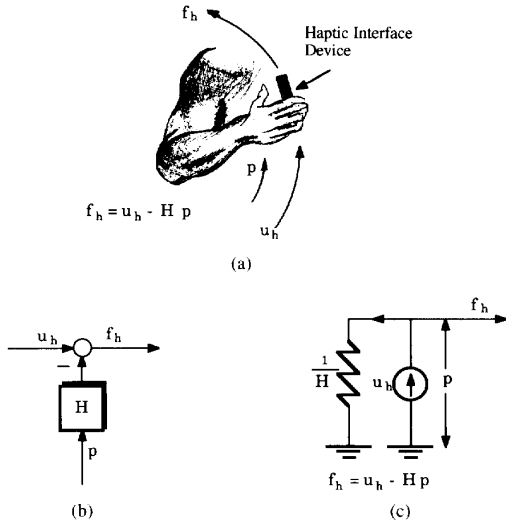


Fig. A1. (a) In constrained movements, the contact force, f_h , is a function of not only u_h , but also of the imposed position constraint, p . (c) represents the Norton equivalent circuit of the dynamics shown in (b). The current, f_h , is a function of not only the current source, u_h , but also of the imposed voltage drop, p .

pin into a wall is an example of a constrained movement where the human imposes a force on the pin, without being concerned with the pin position in the direction normal to the wall; this system may be viewed as one that accepts force commands from the central nervous system. Considering the above dilemma in attributing a particular control action to constrained movements of the human arm, we use a Norton or a Thevenin equivalent concept [27] to arrive at a general substitute for the dynamic behavior of the human arm interacting with the haptic device. In the same way that the choice of a Norton or Thevenin equivalent does not affect the behavior of a circuit in contact with other circuits, our choice in modeling the human arm by a Norton or a Thevenin equivalent has no effect on the arm's interaction with other systems.

Using the "force-current" analogy between electrical and mechanical systems, a Norton equivalent is now chosen to model the human arm's dynamic behavior as a non-ideal source of force interacting with the haptic device. The notion of "non-ideal," as applied here, refers to the fact that the human arm responds not only to descending commands from the central nervous system but also to position constraints imposed by interaction with the haptic interface device. u_h is that part of the contact force that is imposed by the muscles, as commanded by the central nervous system. If the human arm does not move (i.e., the arm position, $p = 0$), the total contact force, f_h , is the same as u_h . However, f_h is also a function of the haptic device position constraint. If the arm moves, (i.e., the device imposes a position constraint on the human arm), the force imposed on the device will differ from u_h . The analogy can be observed from the Norton equivalent circuit shown in Fig. A1(c): The current, f_h , is a function of not only the current source, u_h , but also the external voltage, p . Considering the above analogy, shown in Fig. A1, the contact

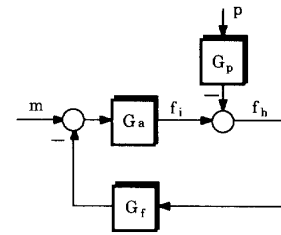


Fig. A2. The internal structure of Fig. A1(b) is presented, where the neural feedback mechanism, G_f , allows for regulation of the contact force, f_h .

force, f_h , can be represented by (A1):

$$f_h = u_h - H(p) \quad (\text{A1})$$

Throughout this article, H is referred to as the human arm impedance and maps the device position constraint onto the contact force. H is determined primarily by the physical and neural properties of the human arm. It will become clear later that H plays an important role in the stability and performance of the system [11]; we will arrive at some experimental values for H in later sections.

Here we give a brief description of the internal structure of the human arm impedance, H , using Fig. A2. Fig. A2 consists of three elements:

- 1) Muscle Activation Dynamics. G_a produces an intended muscle force, f_i , in response to descending neural commands, m .
- 2) Muscular Contraction and Passive Tissue Dynamics. G_p represents the properties of the muscles and passive tissues surrounding the joint and alters the intended force by $G_p p$.
- 3) Neural Feedback. G_f is a feedback operator regulating the force imposed by the human arm on the haptic interface device.

The following discusses briefly the three elements listed above.

B. Muscle Activation Dynamics

G_a represents muscle activation dynamics and maps the descending neural control signals into the intended muscle force, f_i [35]. We rely on this model, since this type of model for muscle activation dynamics has been used with some success in other work [36]. Decoupled operators⁷ for muscle activation dynamics are generally used with Hill-type muscle models [34]. We are interested, however, in the overall behavior of the arm and wish to suppress the details of muscle behavior. Thus, G_a is the only operator we use that explicitly describes muscle behavior. A first order time lag has been suggested in [36] to represent G_a .

C. Muscular Contraction and Passive Tissue Dynamics

G_p is an impedance that reduces the intended force, resulting in the total contact force, f_h . G_p implicitly takes into

⁷Use of a decoupled operator for the activation dynamics implies that muscular activation is assumed to be independent of the muscular contraction process.

account both the internal muscle dynamics, such as the force-velocity and length-tension relationships [8], [24], [33] and the changing effective stiffness of the arm that results from varying the co-contraction of the antagonistic muscles; G_p also includes the dynamic behavior of the passive tissues surrounding the joint. Equation (A2) describes one possible and familiar form for G_p .

$$G_p = Ms^2 + Bs + K \quad (\text{A2})$$

where M represents the mass of the human arm and K and B define the visco-elastic behavior of the muscles and passive tissues.

Note that in the human arm, the descending neural control signals have two functions: (1) causing the arm to move and (2) altering the arm impedance, G_p . Here, we model the first of these functions by m in Fig. A2. The second function, altering the arm impedance, is not explicitly shown but is accounted for in G_p . (See [9] for more information on neurophysiological evidence for the existence of two separate cortical systems, one for determining the commanded limb trajectory, the other for specifying the level of co-contraction.)

D. Neural Feedback

The interaction force, f_h , exerted by the arm on the haptic interface is used as a feedback signal to modulate the descending neural signals. This feedback is effective only at relatively low frequencies because of the limited bandwidth of the central nervous system. Since the human hand can apply very accurately a desired interaction force at very low frequencies, we deduce that G_f is very large at low frequencies. (The experimental results, discussed in later sections, will clarify this.) On the other hand, since the human cannot apply a desired interaction force at high frequencies, G_f must be very small in the high frequency range. Assuming G_f is a linear transfer function, (A3) is a possible choice for G_f .

$$G_f = \frac{C}{s + \lambda} \quad (\text{A3})$$

λ is a scalar representing the bandwidth of the central nervous system and C is a feedback gain. In addition, a pure time delay operator may be introduced in order to account for neural conduction delay.

Simplifying the block diagram shown in Fig. A2 results in the transfer functions shown in Fig. A1.

$$f_h = G_{\text{cns}}m - Hp \quad (\text{A4})$$

where

$$G_{\text{cns}} = \frac{G_a}{1 + G_f G_a} \quad (\text{A5})$$

$$H = \frac{G_p}{1 + G_f G_a} \quad (\text{A6})$$

G_{cns} and H , represent, respectively, the effects of the central nervous system commands and of the haptic device position, p . These operators are shown in Fig. A1 (b) where $u_h = G_{\text{cns}}m$. Note that Fig. A1(b) mathematically represents the closed-loop form of Fig. A2: the force imposed by the human arm

on the device is the result of both the central nervous system commands and the device position constraint. Note that we do not plan to arrive at the values for G_p , G_f and G_a ; we will arrive at a value of H experimentally which contains the effect of G_p , G_f , and G_a implicitly.

A comparison of our modeling approach with that described in [32] clarifies our choice of modeling. In the modeling approach discussed in [32], an interaction force was modeled as the imposed disturbance, while the resultant position was modeled as the feedback variable. This modeling approach is suitable for unconstrained maneuvers. In contrast, in our modeling approach, the interaction force is modeled as the feedback variable, while the position is modeled as the imposed disturbance.

REFERENCES

- [1] H. C. An, G. C. Atkeson, and M. J. Hollerbach, *Model-Based Control of Robot Manipulator*. Cambridge, MA: MIT Press, 1988.
- [2] H. Asada and J. E. Slotine, *Robot Analysis and Control*. New York: Wiley, 1986.
- [3] A. Berthoz and S. Metral, "Behavior of muscular group subjected to a sinusoidal and trapezoidal variation of force," *J. Applied Physiol.*, vol. 29, pp. 378–384, 1970.
- [4] J. D. Cooke, "Dependence of human arm movements in limb mechanical properties," *Brain Res.*, vol. 165, pp. 366–369, 1979.
- [5] J. D. Cooke, "The organization of simple, skilled movements," in *Tutorials in Motor Behavior*, G. Stelmach and J. Requin, Eds. Amsterdam, The Netherlands: Elsevier, 1980.
- [6] C. A. Desoer and M. Vidyasagar, *Feedback Systems: Input-output Properties*. New York: Academic Press, 1975.
- [7] A. G. Feldman, "Functional tuning of the nervous system with control of movement or maintenance," *J. Biophys.*, vol. 11, pp. 565–578.
- [8] A. V. Hill, *First and Last Experiments in Muscle Mechanics*. Cambridge, UK: Cambridge Univ. Press, 1970, pp. 23–41, 124–129.
- [9] D. R. Humphrey and D. J. Reed, "Separate cortical systems for the control of joint movement and joint stiffness: Reciprocal activation and coactivation of antagonist muscles," *Adv. Neurology*, vol. 39, pp. 347–372, 1983.
- [10] J. C. Houk, "Neural control of muscle length and tension," in *Motor Control*, V. B. Brooks, Ed. Bethesda, MD: American Physiological Society Handbook of Physiology.
- [11] H. Kazerooni, "Human-robot interaction via the transfer of power and information signals," *IEEE Trans. Syst. Man Cyber.*, vol. 20, no. 2, 1990.
- [12] H. Kazerooni and S. Mahoney, "Dynamics and control of robotic systems worn by humans," *ASME J. Dynamic Syst., Measurement, and Control*, vol. 133, no. 3, 1991.
- [13] H. Kazerooni, "On the contact instability of the robots when constrained by rigid environments," *IEEE Trans. Automat. Contr.*, vol. 35, no. 3, 1990.
- [14] H. Kazerooni, "On the robot compliant motion control," *ASME J. Dynamic Syst., Measurement, and Control*, vol. 111, no. 3, 1989.
- [15] H. Kazerooni, P. K. Houpt, and T. B. Sheridan, "Fundamentals of robust compliant motion for manipulators," *IEEE Trans. Robotics Automat.*, vol. 2, no. 3, 1986.
- [16] A. J. Koivo and T. H. Guo, "Adaptive linear controller for robotic manipulators," *IEEE Trans. Automat. Contr.*, vol. 28, 1983.
- [17] B. J. Makinson, "Research and development prototype for machine augmentation of human strength and endurance, Hardiman I Project," Rep. S-71–1056, General Electric Co., Schenectady, NY, 1971.
- [18] C. D. Marsden, P. A. Merton, and H. B. Morton, "Stretch reflexes and servo actions in a variety of human muscles," *J. Physiol.*, vol. 259, pp. 531–560.
- [19] M. T. Mason, "Compliance and force control for computer controlled manipulators," *IEEE Trans. Syst. Man Cyber.*, vol. 11, pp. 418–432, 1981.
- [20] N. H. McClamroch and D. Wang, "Feedback control of position and contact force for a two-dimensional mechanism constrained to a given planar contour," presented at Amer. Control Conf., Atlanta, GA, June 1988.
- [21] J. K. Mills and A. A. Goldenberg, "Force and position control of manipulators during constrained motion tasks," *IEEE Trans. Robotics Automat.*, vol. 5, no. 1, 1989.

- [22] N. J. Mizen, "Preliminary design for the shoulders and arms of a powered, exoskeletal structure," Cornell Aeronautical Lab. Rep. VO-1692-V-4, 1965.
- [23] M. H. Raibert and J. J. Craig, "Hybrid position/force control of manipulators," *ASME J. Dynamics Syst. Measurement, and Control*, vol. 102, pp. 126-133, 1981.
- [24] P. M. Rack and D. R. Westbury, "Elastic properties of the cat soleus tendon and their functional importance," *J. Physiol.*, vol. 347, pp. 479-495, 1984.
- [25] D. W. Repperger and A. Morris, "Discriminant analysis of changes in human muscle function when interacting with an assistive aid," *IEEE Trans. Biomed. Eng.*, vol. 35, May 1988.
- [26] K. J. Salisbury, "Active stiffness control of a manipulator in Cartesian coordinates," in *Proc. 19th IEEE Conf. Decision and Control*, Albuquerque, NM, Dec. 1980, pp. 95-100.
- [27] S. D. Senturia and B. D. Wedlock, *Electronic Circuits and Applications*. New York: Wiley, 1975, pp. 51-58.
- [28] T. B. Sheridan and W. R. Ferrell, *Man-Machine Systems: Information, Control, and Decision. Models of Human Performance*. Cambridge, MA: MIT Press, 1974.
- [29] M. W. Spong and M. Vidyasagar, "Robust nonlinear control of robot manipulators," in *Proc. 24th IEEE CDC*, Ft. Lauderdale, FL, Dec. 1985.
- [30] R. B. Stein, "What muscles variables does the nervous system control in limb movements?" *J. Behavioral and Brain Sci.*, vol. 5, pp. 535-577, 1982.
- [31] B. J. Waibel and H. Kazerooni, "On the stability of the constrained robotic maneuvers in the presence of modeling uncertainties," *IEEE Trans. Robotics Automat.*, vol. 7, 1991.
- [32] G. H. Wieneke and J. J. Denier van der Gon, "Variations in the output impedance of the human motor system," *Kybernetik*, vol. 15, pp. 159-178, 1974.
- [33] D. R. Wilkie, "The relation between force and velocity in human muscle," *J. Physiol.*, vol. K110, pp. 248-280, 1950.
- [34] J. M. Winters, "Hill-based muscle models: A systems engineering perspective," in *Multiple Muscle Systems: Biomechanics and Movement Organization*, J. M. Winters and S. L.-Y. Woo, Eds. New York: Springer-Verlag, 1990, pp. 69-93.
- [35] G. I. Zahalak, "Modeling muscle mechanics (and energetics)," in *Multiple Muscle Systems: Biomechanics and Movement Organization*, J. M. Winters and S. L.-Y. Woo, Eds. New York: Springer-Verlag, 1990, pp. 1-23.
- [36] F. Zajac, "Muscle and tendon: properties, models, scaling and application to biomechanics and motor control," *CRC Crit. Rev. Biomed. Eng.*, vol. 17, pp. 359-415, 1989.



Engineering Department and Bioengineering Group at the University of California, Berkeley.

H. Kazerooni received the M.S. degree in mechanical engineering from the University of Wisconsin-Madison in 1980, and the M.S.M.E. and Ph.D. degrees in mechanical engineering from MIT, Cambridge, MA, in 1982 and 1984, respectively.

From 1984 to 1985 he was with the Laboratory of Manufacturing and Productivity at MIT as a Post-Doctoral Fellow. He served at the University of Minnesota, Minneapolis, until 1991, where he held the McKnight-Land Grant Fellowship. He is currently an Associate Professor in the Mechanical and Bioengineering Group at the University of



Ming-Guo Her received the B.S. degree in mechanical engineering in 1983 from Tatung Institute of Technology, Taipei, Taiwan, and both the M.S. and Ph.D. degrees in mechanical engineering from the University of Minnesota, Minneapolis, in 1988 and 1991, respectively.

From 1991 to 1992, he was with the Department of Mechanical Engineering of the University of Minnesota as an Instructor. He is currently an Associate Professor in the Department of Mechanical Engineering at Tatung Institute of Technology. His

research interests include design and control of robotic systems, mechatronic, and machine learning systems.

Dr. Her is a member of the ASME, and is on the Board of Directors of the Chinese Society of Mechatronics and Automation.